Journal of Materials Science & Technology 209 (2025) 95–102

Contents lists available at ScienceDirect

Journal of Materials Science & Technology

journal homepage: www.elsevier.com/locate/jmst

Research Article

High-work-function transparent electrode with an enhanced air-stable conductivity based on AgNiCu core-shell nanowires for Schottky photodiode

Tingting Yan[a,1], Wei Yang[b,1], Limin Wu[a,c,*], Xiaosheng Fang[a,*]

[a] Department of Materials Science, State Key Laboratory of Molecular Engineering of Polymers, Fudan University, Institute of Optoelectronics, Shanghai 200438, China
[b] SINOMACH Intelligence Technology Co., Ltd., Guangzhou 510700, China
[c] College of Chemistry and Chemical Engineering, Inner Mongolia University, Hohhot 010021, China

ARTICLE INFO

Article history:
Received 21 April 2024
Revised 20 May 2024
Accepted 20 May 2024
Available online 27 May 2024

Keywords:
Mental nanowires
Cu-doping
Air-stable conductivity
Transparent electrode
Photodiode

ABSTRACT

Silver nanowires (Ag NWs) have promising application potential in electronic displays because of their superior flexibility and transparency. Doping Ni in Ag NWs has proven to be an effective strategy to improve its work function. However, AgNi NWs-based electrodes suffer from poor electrical conductivity under air exposure due to the low-conductivity NiO generated on its surface. Here, Cu was further doped in AgNi NWs to form AgNiCu NWs and regulate its surface oxide under long-term air exposure. Finally, it is demonstrated that the conductivity of AgNiCu NWs can acquire an improved tolerable temperature (over 240 °C) and prolonged high-temperature tolerance time (over 150 min) by finely regulating the doping content Cu, indicating an enhanced air-stable conductivity. The optimized AgNiCu NWs also achieve superior transparent conductivity as pure Ag NWs and high work function as AgNi NWs, which has been successfully applied in constructing an n-type photodiode with an effective rectification effect.

1. Introduction

Thanks to the boosting requirements of optoelectronics and electronic displays, transparent conductive materials have attracted a lot of research interest [1-5]. Currently, transparent conductive oxides (TCO) like indium tin oxide (ITO) are the most widely used transparent electrodes in traditional display panels or solar cells [6-8]. However, it is difficult for brittle TCO film to form good electrical contact with soft surfaces and surface-structured materials, setting obstacles to its applications in micron- or nano-structured optoelectronic devices and flexible electronics. Flexible transparent conductive materials, including metal nanowires, conductive polymers, carbon nanotubes, and graphene, have the potential to solve this problem [9-12].

Metal nanowires (NWs), typically silver NWs (Ag NWs) or copper NWs (Cu NWs), are regarded as one of the most promising materials in flexible transparent conductors owing to their facile solution-based production, acceptable cost, facilitated morphology control, high optical transparency, low electrical resistance, and good adaptability with flexible structure and surface structured materials [13-15]. Therefore, massive studies have been reported to improve the material properties of metal nanowires or expand their application scope. Most of these reports mainly focus on several aspects: high transparency, low electrical resistance, acceptable cost, and good stability. Nevertheless, the metal-semiconductor contact also needs to be considered besides these parameters, where the work function (W_f) value becomes an important factor [16]. Generally, a good ohmic contact or a strong Schottky barrier in optoelectronic devices requires the W_f value of the electrode material to be either high enough or as low enough to match the Fermi level of the contact semiconductor [10]. However, the most developed Ag NWs and Cu NWs only have moderate W_f values, where neither good ohmic contact nor strong Schottky contact can be formed with many semiconductors.

Fortunately, a surface coating strategy was proposed to modulate the W_f value of transparent Ag NW electrodes in our previous work. Ni-coated Ag NWs were found to successfully inherit the high W_f of nickel, where the AgNi NWs formed an enhanced Schottky barrier with a typical n-type semiconductor [17] and behaved in ohmic contact with p-type material [18]. However, AgNi NWs experience a significant decrease in electrical conductivity, which further weakens upon exposure to air. The square resis-

* Corresponding authors.
[1] These authors contributed equally to this work.
E-mail addresses: lmw@fudan.edu.cn (L. Wu), xshfang@fudan.edu.cn (X. Fang).

https://doi.org/10.1016/j.jmst.2024.05.016
1005-0302/

tance of $AgNi_{0.052}$ (compared at 80 % transmittance) dramatically increases from < 100 to 10^4 Ω sq^{-1} after coating nickel [17], which is only applicable when the operating current is less than 1 pA. This decrease may be attributed to two main factors: firstly, the formation of low-conductivity NiO on the surface upon exposure to air may severely compromise the electrical contact between the metal nanowires; and secondly, the poor crystallization quality of the solution-grown nickel shell could impair conductivity. Therefore, seeking methods to reduce the influence of surface oxidation and promote the shell material's conductivity may break the property limitation of AgNi NWs.

Although the surface oxidation of nickel shells in the air is inevitable, it is possible to improve the electrical conductivity of the NiO layer and restrain its influence. Doping is a common way to improve the conductivity of semiconductor materials, where the dopant donates additional carrier concentration and contributes to enhanced electrical conductivity. As a typical p-type semiconductor, doped NiO materials (e.g. Cu- [19,20], Co- [21], Zn- [22], Al-doped [23]) have been widely used as hole collectors. It has been demonstrated in Chen et al.'s [19] research that the Cu dopant in NiO film effectively increases the W_f value and the conductivity. Inspired by this, introducing Cu dopant into the nickel shell in AgNi NWs may help to reduce the conductivity decrease from surface oxidation. Meanwhile, we found that the melting point of AgNi NWs is considerably enhanced due to the protection of the nickel shell, which can withstand higher temperature annealing to improve crystallization quality and reduce organic residues. In this work, we further introduce copper doping into the nickel shell and improve the electrical properties by annealing. Then a flexible transparent electrode with a high W_f value and enhanced air-stable conductivity was prepared and applied in optoelectronic devices. This work solves the conductivity limitation of high-W_f AgNi NWs and inspires a reasonable route for the conductivity improvement of other core-shell metal nanowires.

2. Experimental section

2.1. Fabrication of metal nanowires

The fabrication of Ag NWs is based on a reduction reaction of silver nitrate. Silver nitrate solution (60 g L^{-1}, ethylene glycol (EG) solvent), polyvinylpyrrolidone (PVP) solution (7.41 g L^{-1}, M_W55000: M_W1300000 = 1:2, EG solvent), and ferric chloride solution (600 μmol L^{-1}, EG solvent) were prepared and mixed in a volume ration of 6:44:5 with fully stirring. The mixed solution was then heated at 140 °C for 3–4 h to finish the growth of Ag NWs, during which the solution turned from transparent to silk gray. 5 mL of the liquid sample was centrifuged at 4500 rpm for 10 min several times (dispersed in ethanol and removed the supernatant) to clean Ag NWs. The cleaned Ag NWs, 2.5 mL PVP solution (2 wt.%, M_W1300000, EG solvent) and 50 μL $Ni_{1-x}Cu_x(NO_3)_2$ solution (0.1 mol L^{-1}, x = 0/0.02/0.04/0.08/0.16, EG solvent) were dissolved and mixed in 12 mL EG, and then 150 μL hydrazine hydrate (50 wt.%) was added to the mixture. After that, the reactants were quickly put in a 120 °C oven for 0.5–1 h to form $Ni_{1-x}Cu_x$ shell on Ag NWs.

2.2. Device construction

The fabricated Ag-$Ni_{1-x}Cu_x$ NWs were centrifuged at 4500 rpm for 10 min several times (dispersed in ethanol and removed the supernatant) before preparing transparent flexible electrodes. Then the Ag-$Ni_{1-x}Cu_x$ NWs were dissolved in ethanol and spray-coated on PDMS films (~2 μm on polytetrafluoroethylene substrates) to form a flexible transparent electrode. Lightly n-type doped silicon wafers were used as photosensitive materials, where the flexible electrode and InGa alloy served as the top electrode and bottom electrode, respectively.

2.3. Material characterization

The transmission electron microscope (TEM) images, along with energy dispersive spectrometer (EDS) mapping, were obtained from a JEM 2100F (JEOL) with EDS attachments. A field emission scanning electron microscope (FESEM, MERLIN Compact, Zeiss) is employed to examine the morphology of the prepared samples, and X-ray diffraction (XRD, Bruker) is used to observe the crystal structure. The inductively coupled plasma mass spectrometry (ICP-MS) test is operated on an Agilent 7700. The XPS data are collected from a PHI5300 (ULVCA-PHI).

2.4. Material calculation

We employed the Vienna Ab Initio Package (VASP) [24,25] to perform all the density functional theory (DFT) calculations within the generalized gradient approximation (GGA) using the PBE [26] formulation. We chose the projected augmented wave (PAW) potentials [27,28] to describe the ionic cores and take valence electrons into account using a plane wave basis set with a kinetic energy cutoff of 400 eV. Partial occupancies of the Kohn-Sham orbitals were allowed using the Methfessel-Paxton smearing method and a width of 0.20 eV. The electronic energy was considered self-consistent when the energy change was smaller than 10^{-5} eV. A geometry optimization was considered convergent when the force change was smaller than 0.02 eV $Å^{-1}$.

2.5. Optical and electrical measurements

A Hitachi U-4100 UV–vis spectrophotometer was used to obtain the absorbance and the transmissivity results. The Fermi levels were calculated from UV photoelectron spectrometer (UPS) data (from an ESCALAB 250Xi, Thermo Fisher). The electrical and photoelectric measurements were operated on a semiconductor characterization system containing a four-probe table, Keithley 4200, Xe lamp, and monochromator. All the photoelectric measurements are operated at room temperature under ambient conditions.

3. Results and discussion

3.1. Morphology and microstructure of AgNiCu NWs

Pure Ag NWs and Ag-$Ni_{1-x}Cu_x$ nanowire samples (abbreviated as ANCa, a = 100x and x refers to the element concentration in the liquid reactant) were prepared as described in the Experimental Section. Fig. 1(a–f) presents TEM and high-resolution transmission electron microscopy (HRTEM) morphology of ANC8 (with the 8% doping content of Cu in Ni-Cu total concentration) and AgNi NWs (ANC0). Basically, ANC0 and ANC8 samples present similar core morphology to pure Ag NWs (Fig. S1 in Supporting Information), where there are coating layers with thicknesses of 2.6 and 2.4 nm on their surface to form core-shell structures (Fig. 1(b, e)). Similar interplanar spacing to pure Ag NWs can be observed in the core of ANC0 and ANC8 samples, here, 2.36 Å is the constant of the Ag (111) in-plane spacing, and 2.04 Å is the constant of the Ag (200) in-plane spacing, indicating that their core is mainly composed of Ag NWs. The interplanar spacing of the surface shell of the ANC0 sample is 1.23 Å (Fig. 1(f)), which is very close to the (220) crystal plane spacing of Ni (JCPDF # 01-1260, $d_{(220)}$ = 1.24 Å), indicating that the shell composition is Ni. In the ANC8 sample, the interplanar spacing of the surface shell material is 1.26 Å (Fig. 1(c)), slightly higher than that of the shell of ANC0 nanowire, which may be due to the dominant substitution doping of Cu on Ni and Cu

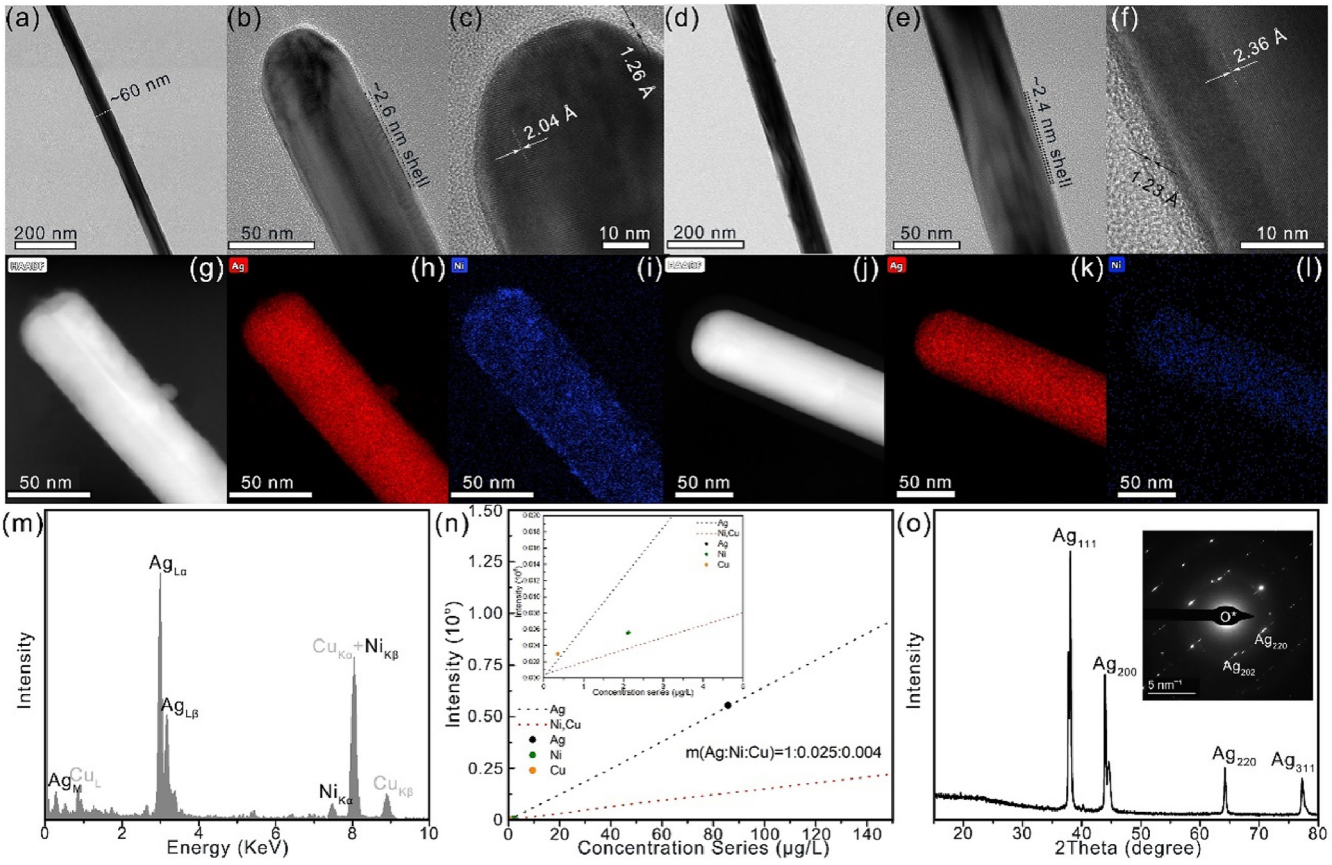

Fig. 1. The TEM and HRTEM images of (a–c) ANC8 and (d–f) ANC0. The elemental mapping results of (g–i) ANC8 and (j–l) ANC0. The EDS (m), ICP (n), and XRD (o) results of the ANC8 sample.

(128 pm) has a slightly higher atomic radius than Ni (124 pm). Cu-Ni alloys exhibit a binary homogeneous phase diagram and Cu element doping will not alter the lattice structure of the shell layer. The HRTEM results of ANC0 and ANC8 samples near the shell layer indicate they are almost composed of a single crystalline grain and have high crystal quality with a consistent crystal orientation (Fig. S2). This is mainly attributed to the similarity between Cu and Ni in terms of electronegativity, atomic radius, and crystal structure. Cu can achieve high solubility in the Ni phase without significantly affecting the crystallization performance of the Ni shell. Even as the Cu element contents in the shell reach 8%, the ANC8 nanowires still maintain high crystallization quality in the shell. In addition, ACN8 adopted the same optimization strategy as ANC0 to introduce ethylene glycol in the original solution to prolong the reaction time and improve the quality of shell crystallization (Figs. S3–S6).

EDS mapping was conducted to demonstrate the elemental distribution of ANC8 and ANC0 (Fig. 1(g–l)). The elemental mapping results of the ANC8 sample are very similar to that of the ANC0 sample, showing a clear Ag-Ni core-shell element distribution, in which the Ag element is concentrated in the center region of the nanowire, while the Ni element mainly distributes on the surface of the nanowire, suggesting Ni element dominates in the shell layer. The EDS data of the ANC8 sample is shown in Fig. 1(m), in which Ag element depicts the strongest elemental peak signal, and the elemental peak corresponding to Ni element can be also observed, however, Cu elemental peak signals in the EDS test are much higher than Ni elemental peak signals, which has an extremely difference from the Cu elemental concentration in the original reaction solution, mainly due to the interference from the Cu mesh substrate during the EDS test.

ICP-MS was further used to accurately determine the content of elemental Cu in ANC8 nanowire samples, as shown in Fig. 1(n). The ANC8 sample is centrifuged several times before testing to remove residual reaction solution byproducts, ensuring that all Cu elements in the sample come from the nanowire structure. The mass ratio of Ag, Ni, and Cu elements was 1:0.025:0.004, from which the chemical composition of the ANC8 nanowire sample was calculated as $AgNi_{4.61\%}Cu_{0.67\%}$, which is close to the elemental concentration in the original reaction solution. The XRD results of the ANC8 sample are shown in Fig. 1(o), where all peaks correspond to the signal of Ag [17] due to the low absolute content of Ni and Cu in the sample thus the main signal peak of Ni and Cu will be swamped by the signal peak of Ag (200).

3.2. High-temperature properties of AgNiCu NWs

Next, to accelerate the oxidation process under air exposure, the resistance and optical properties of Cu-doped ANC8 at high temperatures were investigated in detail, and assess the practical effects of Cu doping in the ANC0 sample. ANC8 and ANC0 present better thermostability than pure Ag NWs which experience a dramatic deterioration of conductivity at around 190 °C, However, the resistance of the ANC0 sample starts to rise after the heating temperature reaches 220 °C, whereas the ANC8 sample presents an improved endurance temperature of 240 °C (Fig. 2(a)), indicating that the conductivity under air exposure may be further improved after Cu-doping in ANC0 sample. Deterioration of conductivity may be due to the surface oxidation of the nanowires becoming severe with the prolongation of accumulated heating time, while the conductivity of CuO on the ANC8 surface is better than NiO on the

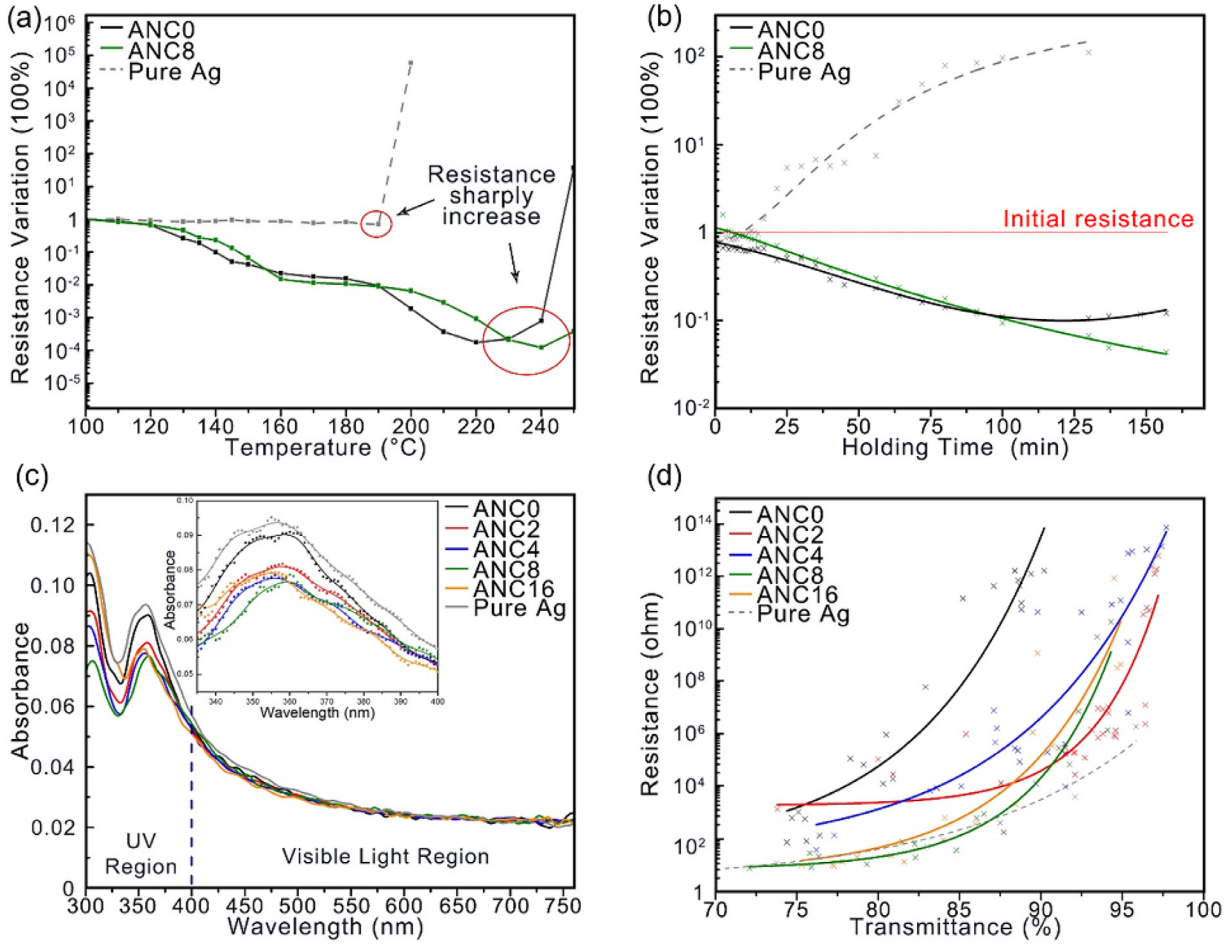

Fig. 2. Resistance variation of ANC0, ANC8, and pure Ag NWs (a) insulated for 20 min at different temperatures and (b) insulation at 185 °C for different times in the air environment. (c) UV–vis absorption curves and (d) resistance-transmittance curves of AgNi NWs with different contents' Cu doping and pure Ag NWs.

ANC0 surface resulting in a better conductivity of ANC8 than ANC0 in high temperature.

In order to further characterize the conductivity stability in air conditions, samples were put at high temperatures (185 °C) with different cumulative heating times (Fig. 2(b)). The resistance of the pure Ag NWs increased rapidly with the heating time, which was due to the low melting point that would disrupt the continuity of the nanowire networks during the heating process. In contrast, the melting points of the ANC0 and ANC8 samples are higher, and the nanowire networks in the ANC0 and ANC8 electrodes may maintain good continuity during the annealing process. The resistance keeps decreasing within a certain holding time because annealing is effective in improving electrical contact between nanowires [29]. However, because samples were heated in air and the surface oxidation rate was fast at 185 °C, the resistance of ANC0 gradually tended to decrease slowly as the oxidized layer accumulated on its surface with heating time increased. When the heating time exceeded 110 min, due to the accumulated high-resistance NiO layer on the ANC0 surface, the resistance of ANC0 began to rise. Due to the higher electrical conductivity of the surface oxidized layer with Cu doping, ANC8's resistance kept decreasing within a longer cumulative heating time (over 150 min) (Fig. 2(b)).

The light absorbance and transmittance of the samples with different Cu doping contents were characterized in detail to assess their potential for practical application as transparent conducting electrodes. As shown in Fig. 2(c), different Ag-based NWs all have low light absorbance in the visible range, whereas there is a characteristic absorption peak in the UV region due to the localized surface plasmon resonance (LSPR) effect of the metal nanowires [30]. Small differences in the light absorbance in the UV region are due to the size changes of the nanowires and the alteration of the surface physicochemical environment with different Cu doping concentrations [31], while the light absorbance in the visible region is almost the same.

Transparent conductivity performance in different samples can be evaluated through the transmittance-resistance curves as shown in Fig. 2(d), where the samples' transmittance was changed by regulating the density of nanowires. Compared with the ANC0, the transparent conductivity of the ANC2, ANC4, ANC8, and ANC16 are significantly improved after Cu doping. When the concentration of Cu is below 8%, the transparent conductivity gradually improves with the increase of Cu concentration, and ANC8 can reach a transparent conductivity comparable to that of pure Ag NWs. As the concentration of Cu is higher than 8%, the transparent conductivity of ANC16 begins to decrease with the increase of Cu content. This suggests that there exists an optimum Cu doping concentration in the Ni-shell layer, which has been commonly proved in doping studies of oxide semiconductors such as NiO [32,33]. At very low doping concentrations, due to the good dispersion of Cu in NiO, Cu atoms tend to contribute additional carriers' concentration as nickel-substituting dopant atoms, and the electrical conductivity of the surface NiO layer rises with increasing Cu-doping concentration [19]. However, in heavily Cu-doped NiO, a considerable number of Cu atoms would aggregate to become second phases such

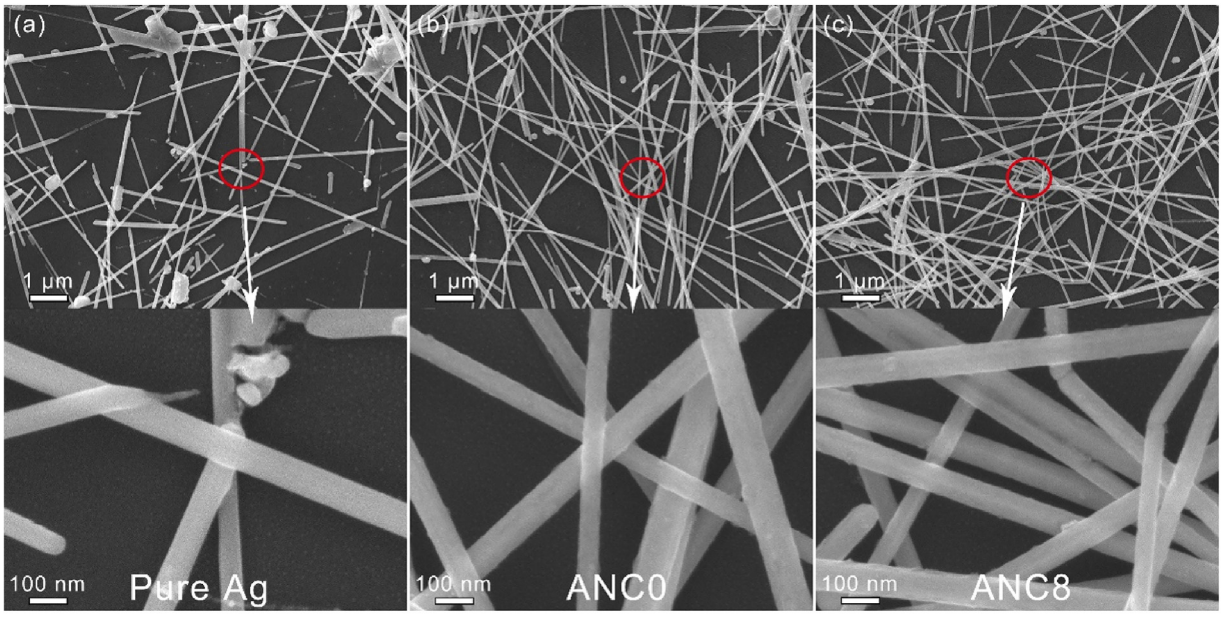

Fig. 3. SEM morphology of pure (a) AgNWs, (b) ANC0 sample, and (c) ANC8 sample after heating for 180 min at 185 °C.

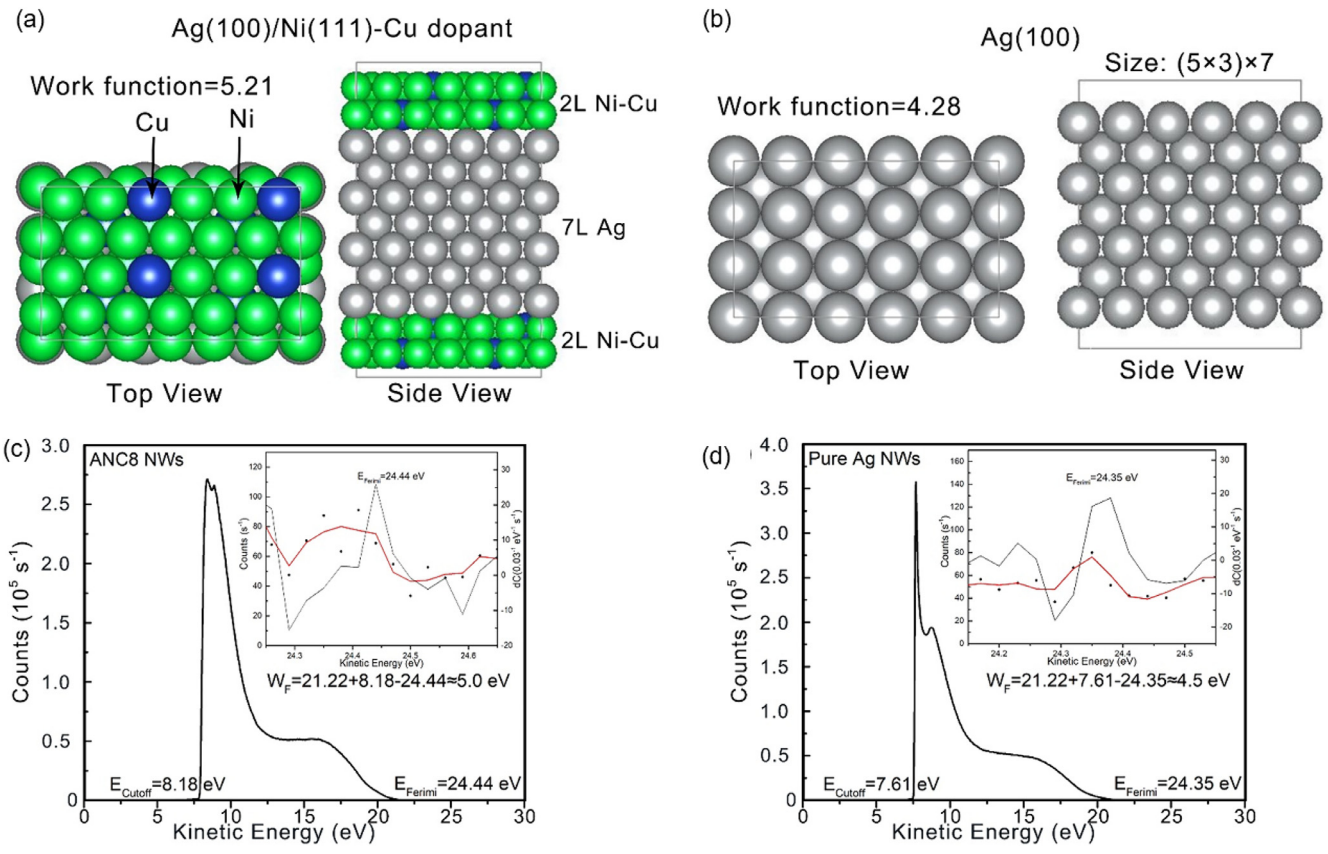

Fig. 4. First-principles calculation of (a) Cu-doped AgNi NWs and (b) pure Ag NWs. UPS results of (c) Cu-doped AgNi NWs and (d) pure Ag NWs.

as copper-oxide not only contributes little to the carrier concentration but also tends to introduce extra defects that will reduce the carrier mobility of NiO.

To further explore the inside reasons for the variability of the electrical conductivity in different samples at high temperatures, the scanning electron microscope (SEM) morphology of the pure Ag NWs, ANC0, and ANC8 nanowire networks was investigated after being heated at 185 °C for 180 min as shown in Fig. 3. Pure Ag NWs presented severe melting fracture after the thermal annealing process, which destroys the continuity of the metal-conducting networks (Fig. 3(a)), and therefore, led to the sharp increase of the Ag NWs in resistance (Fig. 2(a)). In contrast, under the same thermal annealing conditions, no obvious melting fracture was found in the networks of ANC0 and ANC8 nanowires, which still maintained a good continuity (Fig. 3(b, c)). Since the thermal annealing process can effectively improve the quality of electrical contact

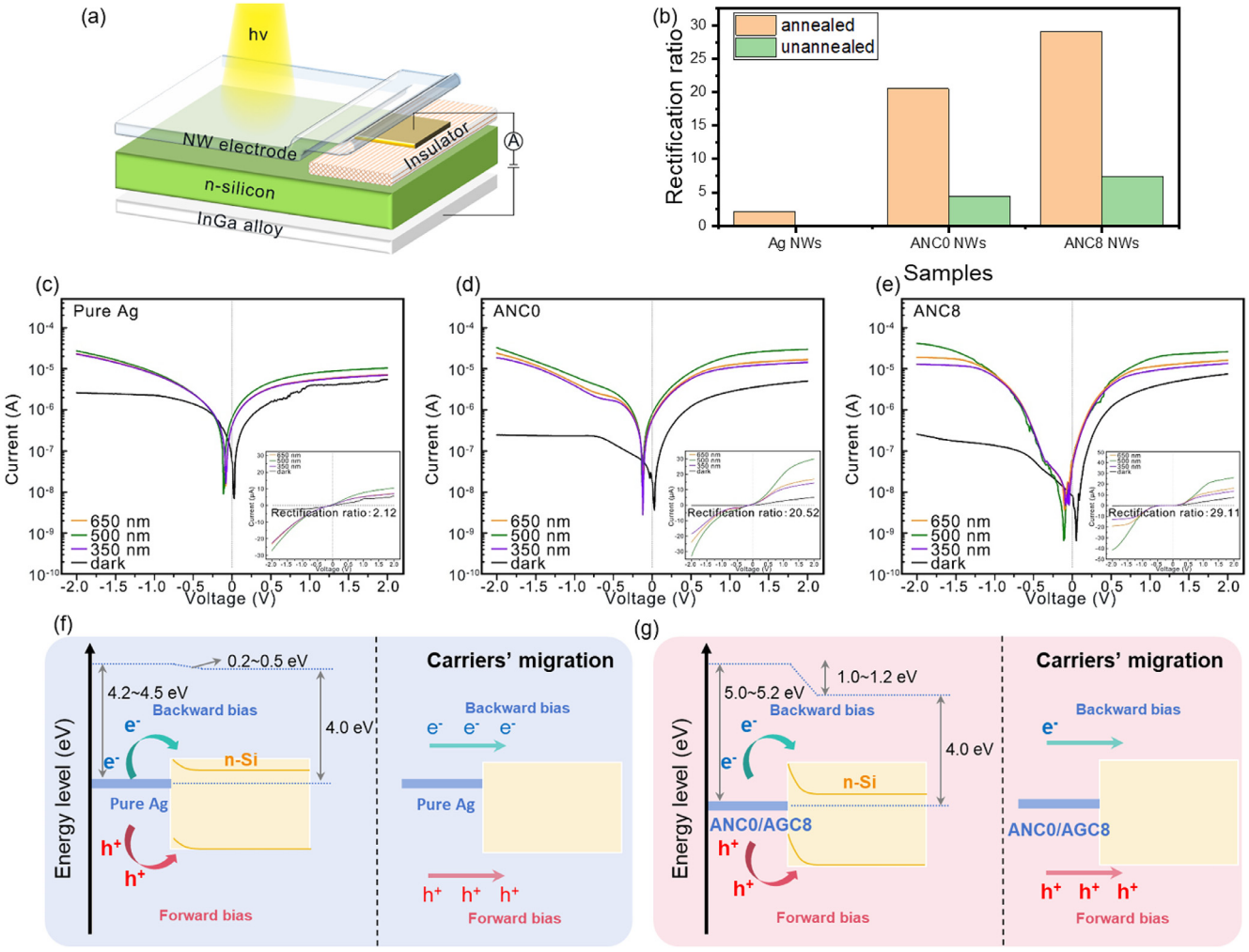

Fig. 5. (a) Schematic diagram of device structure. (b) Rectification ratio of the device with pure Ag NWs, ANC0 NWs, and ANC8 NWs as top electrodes, respectively. *I–V* curves of the device with (c) pure Ag NWs, (d) ANC0 NWs, and (e) ANC8 NWs as top electrodes, respectively. Carriers' migration under forward/backward bias in the device with (f) pure Ag NWs and (g) ANC0 NWs and ANC8 NWs as top electrodes.

between the metal nanowires and reduce the contact resistance, the ANC0 and ANC8 nanowire electrodes obtained better electrical conductivity after annealing (Fig. 2(b)). It can also be further determined that the difference in the critical temperature at which the conductivity of ANC0 and ANC8 samples begins to deteriorate is not due to the fact that the ANC8 nanowire sample can withstand higher annealing temperatures without melting and fracturing. Actually, the melting point of Cu is lower than that of Ni, so, the theoretical melting point of Ni shell material would decrease after Cu doping [34]. Meanwhile, the similar crystalline quality of the shell material in ANC0 and ANC8 samples will not lead to the difference in melting point of the two samples due to the grain size difference [35-37]. The higher critical temperature of the ACN8 sample is due to the higher conductivity of the oxide layer generated on the Ni-Cu-shell surface compared to that on the Ni-shell in the ANC0 sample with the increase of the oxidation accumulation time.

3.3. Work function and application of AgNiCu NWs

Further investigations are carried out on the work function of ANC8 samples to evaluate the Cu-doped ANC8 samples' application potential in high-work function electrodes. First, the theoretical work function value of Cu-doped ANC8 and pure Ag NWs were studied through theoretical analysis and first-principles calculations. Specifically, all density functional theory calculations were performed using the PBE formula in the generalized gradient approximation using VASP, and the projection-enhanced wave potential was chosen to describe the ion nucleus. In the material modeling, a sandwich-type 2D supercell structure is used to approximate the Ag NWs, where the core is represented by seven layers of Ag atoms, and the shell is represented by two layers of Ni-Cu atoms. In order to simplify the primitive cell size of the model, it is assumed that the Cu-doped atoms are regularly distributed in the Ni shell layer and that one out of every six nickel atoms is substitutive doped by Cu atoms, which is illustrated in Fig. 4(a). First-principle calculations show that the theoretical work function of the ANC8 sample is as high as 5.21 eV (Fig. 4(a)), while the theoretical work function of pure Ag NWs is only 4.28 eV (Fig. 4(b)). It indicates that after the Ni shell layer is doped by Cu, the ANC8 can still maintain a theoretically high work function as ACN0 (Fig. S7). Additional results from the UPS (Fig. 4(c)) are carried, the work function ANC8 is about 5.0 eV (Fig. 4(d)), which is much higher than that of about 4.5 eV in Ag NWs (Fig. 4(d)), which is basically consistent with the theoretical calculations shown in Fig. 4(a, b).

It has been determined that the Cu-doped ANC8 sample has an improved air-stable conductivity, and transparent conductivity, as well as maintains high work function. Therefore, the Cu-doped

ANC8 electrode has an application potential in constructing a photodetector, especially in creating Schottky contact in an n-type photodiode. To elucidate the effect of contact between ANC8 and n-type semiconductors on the performance of photodiodes, a photodiode based on n-type lightly doped silicon wafers (n-Si) was constructed. As shown in Fig. 5(a), InGa alloy acted as the bottom electrode, and ANC8, ACN0, and Ag nanowire electrodes acted as the top electrodes. Due to the low work function of InGa alloy, there is almost no Schottky barrier when it contacts with n-Si. Therefore, it can be considered that the difference in rectification effect and photoelectric performance of the device under reverse bias is mainly due to the difference in work function and conductivity of the nanowire electrodes (Fig. 5(b)).

The contact between nanowire electrodes with various work functions and n-Si will produce different rectification effects, mainly due to the different suppression effects on dark current under reverse bias. Here, pure Ag NWs present the lowest work function (4.2–4.5 eV), which is close to the Fermi level of n-Si (4.0 eV), where a stable built-in electric field cannot be formed to suppress the dark current of Ag NWs-based device under reverse bias, thus the device has a high dark current of 2582 nA at –2 V and a rectification ratio of only 2.12 at –2 V/2 V (Fig. 5(c, f)). This also directly leads to a poor light-dark ratio of the device being only about 1.05×10^1. Devices based on high-work-function ANC0 and ANC8 electrodes exhibit improved rectification effects and optoelectronic performance. Specifically, the ANC0-based device and ANC8-based device present a suppressed dark current of 242 and 256 nA at –2 V, correspondingly resulting in an optimized rectification ratio of 20.52 and 29.11 (Fig. 5(d, e)). This is mainly due to the high-work-function ANC0 and ANC8 electrodes can form a high electrode contact potential barrier with n-Si, effectively suppressing the leakage current of the device in the dark state under reverse bias (Fig. 5(g)). The slightly lower performance of ANC0-based devices compared to ANC8 devices is due to ANC8 exhibiting better conductivity than ANC0 electrodes, resulting in slightly higher dark current and superior photocurrent under 500 nm wavelength in ANC8 devices. In addition, the metal nanowire electrodes that have been thermally annealed exhibit better rectification effects and device performance when constructing photodiodes (Figs. 5(b) and S8). It is that thermal annealing can remove molecular adsorption of water and alcohols, improving the contact resistance between nanowires and the contact quality of metal-semiconductor interfaces. Therefore, compared to pure Ag NWs and ANC0-based devices, ANC8 devices have noticeably enhanced optoelectronic performance advantages for constructing p-type Schottky photodiodes due to their high work function and good transparent conductivity.

4. Conclusions

In conclusion, Cu was successfully doped in the shell layer in a core-shell AgNi NWs (ANC0) to form core-shell AgNiCu NWs (ANC8) to effectively improve the air-stable conductivity, which is own to the formation of an oxide layer with better conductivity on Ni-Cu surface. In addition, the ANC8 sample can still maintain the high-work-function property (5.0 eV) as ANC0 and high transparent conductivity as pure Ag NWs, the Schottky diodes based on ANC8 as top electrode achieved a remarkable improvement in rectification ratio (improved by 15 times) and light-dark ratio (improved by 20 times) under reverse bias voltage compared with pure Ag NWs as a top electrode. This is because a stable built-in electric field can be formed to suppress the dark current. Therefore, the Cu-doped ANC8 sample has notable performance advantages and is suitable for application as a transparent-flexible and high-work-function electrode in photodetectors.

Supplementary material associated with this article can be found, in the online version.

Declaration of competing interest

The authors declare that they have no known competing financial interests or personal relationships that could have appeared to influence the work reported in this paper.

CRediT authorship contribution statement

Tingting Yan: Writing – original draft, Methodology, Investigation, Formal analysis, Data curation. **Wei Yang:** Writing – review & editing, Investigation, Formal analysis, Data curation. **Limin Wu:** Writing – review & editing, Conceptualization. **Xiaosheng Fang:** Writing – original draft, Investigation, Funding acquisition, Formal analysis, Conceptualization.

Acknowledgements

The work was supported by the National Natural Science Foundation of China (Nos. 62374035, 92263106, and 12061131009) and the Science and Technology Commission of Shanghai Municipality (No. 21520712600).

Supplementary materials

Supplementary material associated with this article can be found, in the online version, at doi:10.1016/j.jmst.2024.05.016.

References

[1] J.-J. Wang, L.-Z. Feng, G. Shi, J.-N. Yang, Y.-D. Zhang, H. Xu, K.-H. Song, T. Chen, G. Zhang, X.-S. Zheng, F. Fan, Z. Xiao, H.-B. Yao, Nat. Photonics 18 (2023) 200–206.
[2] T. Yan, Z. Li, F. Cao, J. Chen, L. Wu, X.S. Fang, Adv. Mater. 34 (2022) 2201303.
[3] T. Yan, J. Ge, L. Su, X. Liu, X.S. Fang, Nano Lett. 23 (2023) 8295–8302.
[4] T. Yan, Z. Li, L. Su, L. Wu, X.S. Fang, Adv. Funct. Mater. 33 (2023) 2302746.
[5] A. Kumar, S. Rani, N. Chandrakar, D. Sundar Ghosh, Mater. Today: Proc. (2023), doi:10.1016/j.matpr.2023.02.246.
[6] Y. Yun, H. Cho, J. Jung, S.W. Yang, D. Vidyasagar, R.K. Gunasekaran, S. Lee, J. Mater. Sci. Technol. 152 (2023) 100–108.
[7] F. Wang, J. Du, Y. Zhang, M. Yang, D. Han, L. Yang, L. Fan, Y. Sui, Y. Sun, J. Yang, J. Mater. Sci. Technol. 92 (2021) 21–30.
[8] L. Li, W. Shen, C. Yang, Y. Dou, X. Zhu, Y. Dong, J. Zhao, J. Xiao, F. Huang, Y.-B. Cheng, J. Zhong, J. Mater. Sci. Technol. 133 (2023) 145–153.
[9] S. Lee, S. Franklin, F.A. Hassani, T. Yokota, M.O.G. Nayeem, Y. Wang, R. Leib, G. Cheng, D.W. Franklin, T. Someya, Science 370 (2020) 966–970.
[10] Y. Zhou, C. Fuentes-Hernandez, J. Shim, J. Meyer, A.J. Giordano, H. Li, P. Winget, T. Papadopoulos, H. Cheun, J. Kim, M. Fenoll, A. Dindar, W. Haske, E. Najafabadi, T.M. Khan, H. Sojoudi, S. Barlow, S. Graham, J.-L. Brédas, S.R. Marder, A. Kahn, B. Kippelen, Science 336 (2012) 327–332.
[11] J. He, C. Lu, H. Jiang, F. Han, X. Shi, J. Wu, L. Wang, T. Chen, J. Wang, Y. Zhang, H. Yang, G. Zhang, X. Sun, B. Wang, P. Chen, Y. Wang, Y. Xia, H. Peng, Nature 597 (2021) 57–63.
[12] C. Xie, Y. Liu, W. Wei, Y. Zhou, Adv. Funct. Mater. 33 (2023) 2210675.
[13] X. Li, Y.J. Fan, H.Y. Li, J.W. Cao, Y.C. Xiao, Y. Wang, F. Liang, H.L. Wang, Y. Jiang, Z.L. Wang, G. Zhu, ACS Nano 14 (2020) 9605–9612.
[14] Z. Jiang, M.O.G. Nayeem, K. Fukuda, S. Ding, H. Jin, T. Yokota, D. Inoue, D. Hashizume, T. Someya, Adv. Mater. 31 (2019) 1903446.
[15] A. Kumar, A. Sharma, Y. Chen, M.M. Jones, S.T. Vanyo, C. Li, M.B. Visser, S.D. Mahajan, R.K. Sharma, M.T. Swihart, Adv. Funct. Mater. 31 (2021) 2008054.
[16] J. Chen, X. Liu, Z. Li, F. Cao, X. Lu, X.S. Fang, Adv. Funct. Mater. 32 (2022) 2201066.
[17] W. Yang, Y. Zhang, Y. Zhang, W. Deng, X.S. Fang, Adv. Funct. Mater. 29 (2019) 1905923.
[18] W. Yang, K. Hu, F. Teng, J. Weng, Y. Zhang, X.S. Fang, Nano Lett. 18 (2018) 4697–4703.
[19] W. Chen, Y. Wu, J. Fan, A.B. Djurišić, F. Liu, H.W. Tam, A. Ng, C. Surya, W.K. Chan, D. Wang, Z.-B. He, Adv. Energy Mater. 8 (2018) 1703519.
[20] A. Liu, H. Zhu, Z. Guo, Y. Meng, G. Liu, E. Fortunato, R. Martins, F. Shan, Adv. Mater. 29 (2017) 1701599.
[21] Y. Xie, K. Lu, J. Duan, Y. Jiang, L. Hu, T. Liu, Y. Zhou, B. Hu, ACS Appl. Mater. Interfaces 10 (2018) 14153–14159.
[22] X. Wan, Y. Jiang, Z. Qiu, H. Zhang, X. Zhu, I. Sikandar, X. Liu, X. Chen, B. Cao, ACS Appl. Energy Mater. 1 (2018) 3947–3954.
[23] B. Parida, S. Yoon, J. Ryu, S. Hayase, S.M. Jeong, D.W. Kang, ACS Appl. Mater. Interfaces 12 (2020) 22958–22970.
[24] G. Kresse, J. Furthmüller, Comput. Mater. Sci. 6 (1996) 15–50.
[25] G. Kresse, J. Furthmüller, Phys. Rev. B 54 (1996) 11169–11186.
[26] J.P. Perdew, K. Burke, M. Ernzerhof, Phys. Rev. Lett. 77 (1996) 3865–3868.

[27] G. Kresse, D. Joubert, Phys. Rev. B 59 (1999) 1758–1775.
[28] P.E. Blöchl, Phys. Rev. B 50 (1994) 17953–17979.
[29] M. Kaikanov, A. Kemelbay, B. Amanzhulov, G. Demeuova, G. Akhtanova, F. Bozheyev, A. Tikhonov, Nanotechnology 32 (2021) 145706.
[30] S. Bae, H. Han, J.G. Bae, E.Y. Lee, S.H. Im, D.H. Kim, T.S. Seo, Small 13 (2017) 1603392.
[31] H. Yin, Y. Zhao, X. Xu, J. Chen, X. Wang, J. Yu, J. Wang, W. Wu, ACS Omega 4 (2019) 14404–14410.
[32] Y. Kokubun, S. Nakagomi, Phys Status Solidi B 257 (2020) 2000330.
[33] S. Hartner, M. Ali, C. Schulz, M. Winterer, H. Wiggers, Nanotechnology 20 (2009) 445701.
[34] A. Muntean, M. Wagner, J. Meyer, M. Seipenbusch, J. Nanopart. Res. 18 (2016) 229.
[35] Y.H. Chen, L.X. Su, M.M. Jiang, X.S. Fang, J. Mater. Sci. Technol. 105 (2022) 259–265.
[36] J. Liu, X. Fan, Y. Shi, D.J. Singh, W. Zheng, J. Phys. Chem. C 123 (2019) 907–914.
[37] T. Wejrzanowski, M. Lewandowska, K. Sikorski, K.J. Kurzydlowski, J. Appl. Phys. 116 (2014) 164302.